Crack Trajectories in Ductile Materials Under Unsymmetric Conditions: Theory and Numerical Simulation

M. M. Rashid[1] and V. Tvergaard[2]

[1]Department of Civil and Environmental Engineering
University of California, Davis
Davis, CA 95616 USA

[2]Department of Mechanical Engineering
Technical University of Denmark
2800 Kgs. Lyngby, Denmark

ABSTRACT. *A 2D computational model of ductile fracture, in which arbitrary crack extension through the mesh is accommodated without mesh bias, is used to study ductile fracture near the weld line in welded aluminum plates. Comparisons of the calculated toughness behavior and crack trajectory are made with results found in the literature.*

INTRODUCTION

Weldments in metals represent complex, often fracture-critical situations, with high residual stresses, sharply graded material properties, and sometimes pre-existing damage all contributing to the overall structural behavior. Because the fracture resistance usually varies markedly within and near the weld line, the tendency of a crack to deviate either toward or away from this zone can have significant consequences for the overall toughness of the welded structure. Modeling of fracture in welded structures is complicated not only by the presence of (typically) significant ductility, but also by the many sources of asymmetry, making a robust crack-direction criterion a necessity.

Fracture modeling in the presence of significant plastic flow represents a considerable challenge, particularly when the crack path is not dictated by symmetry. Cohesive-zone ideas have been used by many authors [1-3] with some success, although the suitability of this approach when the crack path is unknown *a priori* is far from clear. Also, local damage models coupled with the finite element method, in which element deletion is made to occur when the damage level reaches a prescribed threshold, continue to be used to simulate rupture in ductile materials [4, 5].

In this paper, a novel modeling approach to fracture in 2D domains is employed to study a problem involving weldments in aluminum alloy plates. The modeling approach and its computational embodiment are briefly described in the following two sections. A major feature of the model is its ability to accurately resolve the angular dependence of the near-tip fields, making it well-suited to unsymmetric fracture scenarios that exhibit kinking or curved crack trajectories. The model problem presented

below corresponds to the experiments performed by Nègre et al. [6, 7], which involved compact-tension specimens machined from welded aluminum plates.

FRACTURE MODEL

In the present work, a fracture-modeling framework proposed in [8, 9] is used to study curvilinear crack growth in a heterogeneous ductile metal. This theory, called the "exclusion region" (ER) theory, is based on special treatment of a small material region that contains the current crack tip. This region is circular in the undeformed reference configuration, with the crack tip at its center (Figure 1). The ER theory embodies two major elements: 1) a characterization of the mechanical behavior of the exclusion region, and 2) a criterion for the advance of the crack tip – and its surrounding exclusion region with it – through the material. With regard to the first of these, the view is taken that, very near the crack tip, deformation processes occur which are not easily represented by standard continuum kinematics. Accordingly, the displacement field within the ER is assumed to take the form

$$\mathbf{u} = \hat{\mathbf{u}}(\vartheta)\,\xi + (1-\xi)\mathbf{g} - \xi(1-\xi)\,\mathrm{v}\mathbf{M}(\vartheta)\,, \quad \xi = \frac{r}{a}\,, \tag{1}$$

where (r, ϑ) are polar coordinates in the reference configuration with current crack tip as origin, $r = a$ defines the boundary between the exclusion region and the bulk continuum, $\hat{\mathbf{u}}(\vartheta)$ is the displacement at the ER/bulk-continuum interface, and $\mathbf{M}$ is the unit tangent vector on the ER boundary. Equation (1) specifies a near-tip displacement field which is controlled by the interface distribution $\hat{\mathbf{u}}(\vartheta)$, the tip displacement $\mathbf{g}$, and the additional scalar parameter v. A single discontinuity in the ER-boundary displacement $\hat{\mathbf{u}}(\vartheta)$ is admitted, corresponding to separation of the crack faces.

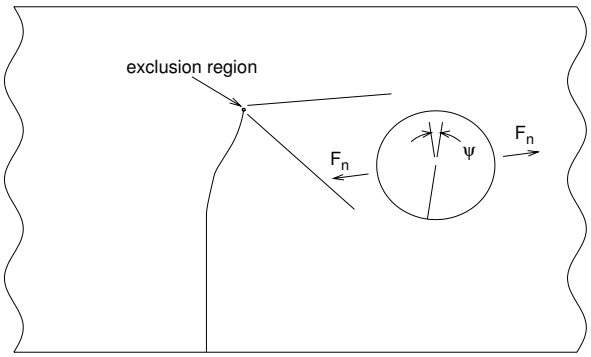

Figure 1. The crack-tip exclusion region.

No claim is made that (1) is an accurate representation of the actual near-tip displacement field. Rather, the role of (1) in the theory is to provide the necessary kinematics at the ER boundary so that the material state can be evaluated, using the bulk constitutive

model. With the material state, and therefore the stress, known on the ER boundary, the traction is easily evaluated. An overall force and moment equilibrium requirement is imposed on the traction distribution at $r = a$, providing three conditions for the determination of the internal displacement parameters $\mathbf{g}$ and v. The assumed form (1) thereby facilitates a *generalized constitutive model* for a finite-size material region that contains the crack tip – "generalized" because, unlike the local constitutive model from which it emerges, it admits a crack-like displacement discontinuity. It is shown in [8] that this generalized constitutive model reduces to a finite-volume version of the prevailing local model in the absence of a displacement discontinuity.

The second element of the ER theory, namely the criterion for advancing the crack, takes the simple form $\text{Max}\ \Phi = \Phi_c$. Here, the *separation function* Φ is a function of the material state on the exclusion-region boundary, along with a *candidate direction of advance* ψ. Φ_c is a material-dependent critical value. In order to realize quasistatic (i.e. stable) crack growth, the remote loading must be controlled in such a manner that the above criterion is continuously satisfied. The direction of advance is then given by the angle ψ that maximizes the separation function. The separation function may depend on the material state at $r = a$ in an arbitrary way, and should be designed to reflect the material's propensity to separate on a plane given by the orientation ψ.

A simple separation function, suitable for brittle materials, is given in [8]. The ductile fracture scenarios considered in [10, 11], on the other hand, were modeled by making the separation function sensitive to both the resultant normal-opening force acting on the ER, as well as the intensity of the plastic strain. Here, in an effort to better fit the experimental results of Nègre et al. [6, 7] discussed later, a different separation function is proposed. With reference to Fig. 1, this separation function is given by

$$\Phi(\psi) = \frac{\varphi\, D(\psi)}{\underset{\psi}{\text{Max}}\, D(\psi)}\,, \quad D(\psi) = \int_0^{2\pi} H(2\pi - \vartheta + \psi)\, H(\vartheta - \psi)\, \sin^2(\vartheta - \psi)\, \varepsilon(a, \vartheta)\, \mathrm{d}\vartheta\,. \tag{2}$$

The direction-dependence of this separation function is given by a weighted average of the equivalent plastic strain ε on the exclusion-region boundary, whereas the magnitude of the separation function is determined by the ER opening angle. In unsymmetric situations, the direction function $D(\psi)$ favors crack extension toward the region of more intense plastic flow. The separation function (2) might be regarded as an unsymmetric generalization of the crack-tip opening angle (CTOA) criterion, which, although distinctly phenomenological in nature, has met with considerable success in modeling ductile fracture [12].

COMPUTATIONAL APPROACH

Even in two dimensions, high-fidelity simulation of unsymmetric fracture processes presents some interesting challenges, particularly when fracture is accompanied by significant plastic flow. In particular, some form of stepwise redesign of the spatial discretization is generally required in order to realize sufficiently accurate resolution of the

near-tip fields, while at the same time accommodating the geometrically arbitrary, and *a priori* unknown, crack path. This requirement in turn engenders the need for a supporting material-state remapping procedure, whereby the solution state is transferred from one mesh to the next. It is remarked that fracture problems present particularly demanding applications in this regard, for two reasons: first, the mesh must be redesigned, and therefore the solution must be transferred, on *every increment* of crack extension and not merely a few times during the course of the analysis; and second, the fields exhibit high curvature in the very place where accurate remapping is most critical – near the crack tip.

A finite-element-based computational approach is taken here, in which the crack trajectory is accommodated with a circular *moving mesh patch* (Figure 3). The mesh patch is automatically generated on every step along the crack path, and consists of annular rings of four-node quadrilateral elements surrounding the exclusion region. As can be seen from Figure 3, the patch is in general incompatible with the background mesh, necessitating a weak enforcement of displacement compatibility across the interface. Such a scheme is described in [13]. In this scheme, the standard nodal equilibrium equations are appended with a set of compatibility equations, whose conjugate unknowns relate to the equal-and-opposite traction distribution that must be applied across the patch-background interface.

The incompatible-mesh-patch method provides a highly refined, uniform mesh environment in the near-tip region, in which a high level of mesh resolution is evident in the circumferential direction. This is important for accurate determination of the crack trajectory. As the crack is advanced, the mesh patch is generated anew at each new crack-tip location, and the material state (Cauchy stress and equivalent plastic strain) is mapped from the old mesh to the affected elements in the new mesh. The transfer operator proposed in [14] is used, which amounts to weak enforcement of equality between the quadrature-point fields in the new and old meshes.

A MODEL PROBLEM: ALUMINUM WELD

A thorough study of fracture in butt welds of aluminum 6000-series alloy plates was recently published by Nègre and coworkers [6, 7]. In this study, CO_2 laser-beam welding was used to join the aluminum alloy plates, with tensile-test and compact-tension specimens being cut at various locations relative to the weld line. A fusion zone of width 2.8mm was identified by means of microhardness measurements, with a heat-affected zone of width 9mm on either side of the fusion zone. Outside the heat-affected zone, the material properties were those of the base metal.

The uniaxial stress-strain response of the weldment was measured with fairly fine spatial resolution by machining tensile specimens, in the form of flat strips with 2mm $\times$ 0.5mm cross section, at 0.84mm intervals parallel to the weld line. The compact-tension specimens were of standard configuration, with $a/W = 0.5$, $W = 50$mm, and $B = 4.2$mm. Three different CT configurations were tested: configuration BM, which consisted of homogeneous base metal; FZ, in which the symmetry line of the specimens

coincided with the middle of the fusion zone; and HAZ, in which the symmetry line lies at the interface between the fusion zone and the heat-affected zone. Configurations BM and FZ are geometrically and materially symmetric, and would therefore be expected to exhibit self-similar crack growth. On the other hand, the geometric symmetry line in the HAZ configuration is parallel to, but displaced 1.4mm from, the center of the fusion zone. This material asymmetry caused the crack path to deviate toward the fusion zone.

A companion modeling effort was undertaken by Nègre et al. [6, 7], in which two different approaches were taken. In one, a dilatant plasticity/damage model [15] was used in a 3D finite element program to simulate the behavior of the CT fracture specimens. In this model, only the fusion zone was modeled with the damage formulation; the remainder of the specimen was taken to consist of a standard J_2 flow-theory elastic-plastic material. A (fixed) 3D finite element mesh was used with a high degree of spatial refinement along the crack path. Because the dilatant-plasticity constitutive model exhibits softening, localization is a feature of the solutions, thereby introducing mesh-dependence into the predictions. The material constants for the Tvergaard-Gurson-Needleman constitutive model were fixed through a calibration procedure using the tension-strip specimens. The fracture-specific parameters in the model, in particular the critical void-volume fraction at which the crack was extended by deleting elements from the mesh, were determined by fitting the force-CMOD data for the BM and FZ fracture specimens. As can be seen from Figs. 7 and 8 of [7], a good match was obtained between the experimental and computational results for these symmetric specimens.

In their analyses of the (materially unsymmetric) HAZ specimens, Nègre and coworkers [7] underpredicted the peak opening force, but came much closer to reproducing the experimental force-CMOD curve when a layer of higher-flow-strength material was inserted at the interface between the fusion zone and the heat-affected zone. Also, prediction of the experimentally-observed deviation of the crack path into the fusion zone was found to be quite sensitive to the constitutive parameters. Similarly, the crack trajectory in the second modeling approach [6], which featured a cohesive-zone fracture model in conjunction with a 2D plane-stress representation of the CT specimen with plane-strain core [16], was also found to be rather sensitive to the mesh design.

In the present work, the above-described numerical implementation of the exclusion-region framework was used to simulate the weldment-fracture experiments presented in [6, 7]. The specific fracture model used herein is given by eqn. (2). In the calculations presented below, the ER boundary was discretized into 32 equi-angular segments in order to provide high angular resolution of the near-tip fields. The directional dependence of the separation function (2) is appropriate for situations in which rupture is strongly correlated with the intensity of plastic flow. See [12] for a discussion of the CTOA fracture criterion, of which the present separation function is a generalization.

Following [6, 7], the bulk constitutive model was first calibrated based on the tension-strip stress-strain measurements, and then the fracture-specific material constants were set by fitting CT analysis results to the BM and FZ experimental observations. With regard to the former, the material was taken to be a J_2-flow theory elastic-plastic material with isotropic hardening, where the hardening parameters varied from those of the base metal, through the heat-affected zone, and finally into the fusion zone. The

yield stress was taken to be $Y = Y_0 + Y_1 \varepsilon^n$. The constants Y_0, Y_1, and n were fit by calibrating the calculated uniaxial stress-strain behavior to the test results reported in Figure 8 of [6]. The values are given in Table 1. Notably, the flow strength was found to vary markedly through the heat-affected zone, with a minimum value at the center of this zone and nearly identical values at the interfaces with both the fusion zone and the base metal. The finite element simulations of the CT tests featured continuously graded material properties in accord with these observations.

Table 1. Material properties in the heterogeneous CT specimens.

material property	base material	fusion zone	HAZ (center)	HAZ (at FZ)
Y_0 (MPa)	150.0	145.0	112.5	145.0
Y_1 (MPa)	180.3	250.0	135.2	180.3
n	0.020	0.250	0.020	0.020
ER radius (mm)	0.10	0.10	0.10	0.10
Φ_c (rad)	0.145	0.082	0.118	0.082

The fracture-specific parameters in the present model are only two in number: the exclusion-region radius a, and the critical separation-function value Φ_c, which is equivalent to the critical ER-opening angle. In an effort to represent crack-tip constraint effects as faithfully as possible in these 2D analyses, a variation of the "plane-strain core" idea [16] was employed, whereby the in-plane stress response was taken to be a weighted average of the plane-stress and plane-strain values. The weighting was taken to vary linearly from pure plane strain at the exclusion region, to pure plane stress at and outside a radius equal to the specimen thickness (4.2mm). The overall results were found to depend only weakly on the radius of this "mixed" region.

Preliminary analyses were undertaken to fix the critical opening angle Φ_c in both the base metal and the fusion zone. Specifically, finite element analyses of the homogeneous BM specimen and the graded FZ specimen were performed in which the crack was extended, and the applied load was controlled, in such a manner that the force-CMOD curves reported in [7] were exactly reproduced. This exercise produced opening-angle vs. crack extension curves that generally increased for about the first 2.5 mm of crack extension, after which the opening angle remained roughly constant. The Φ_c values used in subsequent analyses were chosen as the greatest lower bounds in this steady-state regime. Comparisons between the experimental (as reported in[7]) and calculated force-CMOD behaviors are shown in Figure 2. From the figure, it is seen that the peak loads are predicted within a few percent for both the BM and FZ specimens. However, the CMOD values at which these peak loads occur are underpredicted by 22.5% in the FZ case and 14.4% in the case of the BM specimen.

After setting the fracture-related material parameters based on the BM and FZ specimens, the unsymmetric HAZ configuration was then analyzed with no further adjustments to either bulk-material or fracture constants. The predicted and measured force-CMOD curves are shown in Figure 2, from which it is seen that peak load is

underpredicted. An even lower peak load was predicted in the modeling work reported in [7], which compelled these authors to insert a higher-strength layer between the base material and the heat-affected zone, as mentioned previously.

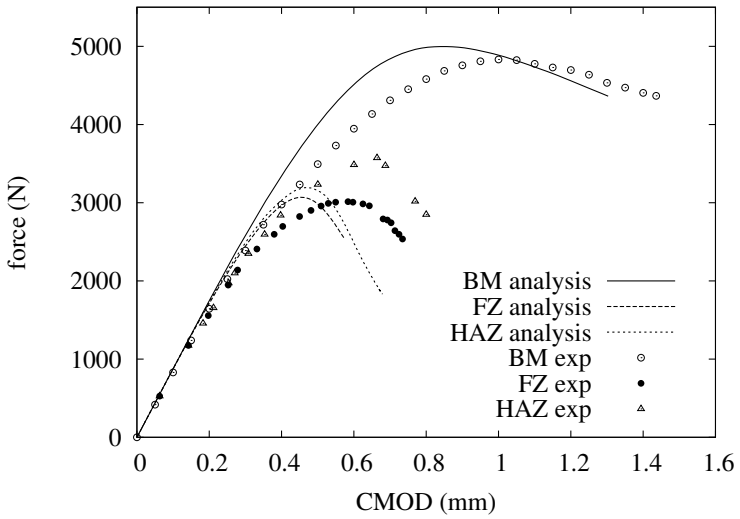

Figure 2. Experimental and calculated force vs. CMOD curves for BM, FZ, and HAZ compact tension fracture specimens.

A deformed mesh and a deformed outline, showing the crack trajectory, are illustrated in Figure 3. In these analyses, plastic flow is confined to a region fairly close to the crack tip, although it is sufficiently intense to strongly affect the near-tip fields. The calculated crack-path deviation averages 17.3° until the crack reaches the center of the fusion zone, which compares well to the experimental average of 17° reported in [6]. Thereafter, in the analysis the crack begins to turn parallel to the weld line.

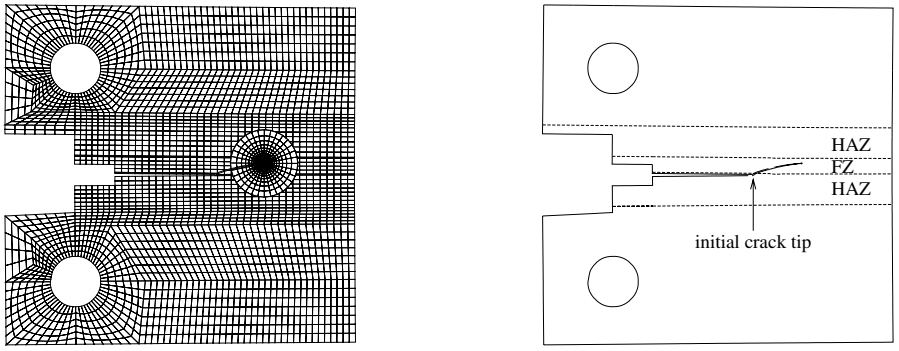

Figure 3. Deformed mesh, and deformed outline showing crack trajectory for HAZ specimen.

CONCLUSION

The discrepancy seen between experimental and calculated CMOD at peak load for all three analyses – BM, FZ, and HAZ (see Fig. 2) – seems to relate to the fact that crack extension apparently begins much earlier in the experiments than it does in the analyses: when the experimental force-CMOD curves first deviate from their projected fixed-crack slopes, all fracture-related parameters – near-tip plastic strain, opening angle, etc. – in the analyses are relatively small and sharply on the rise. This scenario appears to offer little hope that selection of a different separation function, or indeed even a different bulk constitutive model, would entirely remove the discrepancy in peak-load CMOD. Accordingly, it seems likely that a primary cause for this difference is the 2D nature of the calculations. The extensive tunneling shown in Figure 6 of [7] supports this conclusion. The rather severe underprediction of the peak load in the case of the unsymmetric HAZ specimen may well result from a complex distribution of material properties at the interface between the heat-affected zone and the base material. This is suggested by Nè gre et al. [7] in connection with their modeling efforts.

REFERENCES

1. Siegmund, T and Brocks, W (2000) *Eng. Fracture Mech.* **67**, 139-154.
2. Keller, K, Wiehe, S, Siegmund, T, and Kroplin, B (1999) *Comp. Mat. Sci.* **16**, 267-274.
3. Tvergaard, V and Hutchinson, JW (1996) *Int. J. Solids Struct.* **33**, 3297-3308.
4. Gao, XS, Faleskog, J, and Shih, CF (1998) *Int. J. Fracture* **89**, 375-398.
5. Gullerud, A, Gao, X, Haj-Ali, R, and Dodds Jr., RH (2000) *Eng. Fracture Mech.* **66**, 65-92.
6. Nè gre, P, Steglich, D, and Brocks, W (2005) *Int. J. Fracture* **134**, 209-229.
7. Nè gre, P, Steglich, D, and Brocks, W (2004) *Eng. Fracture Mech.* **71**, 2365-2383.
8. Rashid, MM (1997) *Int. J. Solids Struct.* **34**, 2303-2320.
9. Rashid, MM and Roy, R (1999) In: *Fatigue and Fracture Mechanics: Twenty-Nineth Volume, ASTM STP 1332,* 264-283, Panontin, TL and Sheppard, SD (Eds.), American Society for Testing and Materials, West Conshohocken, PA.
10. Rashid, MM and Tvergaard, V (2003) *Int. J. Solids Struct.* **40**, 2819-2831.
11. Rashid, MM and Tvergaard, V (2004) *Int. J. Comp. Eng. Sci.* **5**, 781-794.
12. Newman, JC, James, MA, and Zerbst, U (2003) *Eng. Fracture Mech.* **70**, 371-385.
13. Rashid, MM (1998) *Comp. Meth. Appl. Mech. Eng.* **154**, 133-150.
14. Rashid, MM (2002) *Int. J. Numerical Meth. Eng.* **55**, 431-450.
15. Tvergaard, V (1982) *J. Mech. Phys. Solids* **30**, 399-425.
16. Newman, JC, Booth, BC, and Shivakumar, KN (1988) In: *Eighteenth National Symposium on Fracture Mechanics, ASTM STP 1332,* 665-685, American Society for Testing and Materials, Philadelphia, PA.